

**Optical phonon lineshapes and transport in metallic carbon nanotubes under high bias voltage**

Jürgen Dietel

*Institut für Theoretische Physik, Freie Universität Berlin, Arnimallee 14, D-14195 Berlin, Germany*

Hagen Kleinert

*Institut für Theoretische Physik, Freie Universität Berlin, Arnimallee 14, D-14195 Berlin, Germany  
and ICRAneT, Piazzale della Repubblica 1, 10-65122 Pescara, Italy*

(Received 13 July 2010; revised manuscript received 4 October 2010; published 19 November 2010)

We calculate the current-voltage characteristic of metallic nanotubes lying on a substrate at high bias voltage showing that a bottleneck exists for short nanotubes in contrast to large ones. We attribute this to a redistribution of lower-lying acoustic phonons caused by phonon-phonon scattering with hot optical phonons. The current-voltage characteristic and the electron and phonon distribution functions are derived analytically, and serve to obtain in a self-contained way the frequency shift and line broadening of the zone-center optical phonons due to the electron-phonon coupling at high bias. We obtain a positive offset on the zero bias shift and no broadening of the optical phonon mode at very high voltages, in agreement with recent experiments.

DOI: [10.1103/PhysRevB.82.195437](https://doi.org/10.1103/PhysRevB.82.195437)

PACS number(s): 63.22.Gh, 78.30.Jw, 73.63.Fg, 73.50.Fq

**I. INTRODUCTION**

Carbon nanotubes are one of the strongest and stiffest materials which can sustain very high currents before breaking. This electric property makes metallic nanotubes an interesting alternative to nanometer-sized metallic wires. Since nanotubes can behave like semiconductors, their possible use in logic electronic circuits is promising. This has recently led to a number of experiments evaluating their current vs voltage characteristic at high bias voltage,<sup>1-9</sup> with related theoretical work in Refs. 10-15.

At low voltage, the current-voltage characteristic is mainly influenced by acoustic phonons and by impurity scattering. At higher voltage, optical phonons become important. For metallic nanotubes on a substrate, the current vs voltage curve is increasing, in contrast to suspended nanotubes where the characteristic shows a negative differential conductivity at high bias.<sup>5</sup>

We shall review in Sec. II the current-voltage characteristic of metallic nanotubes lying on a substrate. Following Refs. 11 and 12 we use a Boltzmann approach for the electrons coupled to zone-center and zone-boundary optical phonons. We take into account explicitly the dynamics of the phonons by a Boltzmann equation containing an inelastic term to describe the decay of optical phonons into underlying acoustic phonons.<sup>11,12</sup> We use first the so-called single-mode relaxation time approximation for the scattering term.<sup>16</sup> This is characterized by a thermal phonon relaxation time  $\tau_{\text{op}}$ . For the electron-phonon relaxation time  $\tau_{\text{ep}}$  we use a numerically determined value,<sup>10,17</sup> which reproduce very well the experimentally determined lifetimes of optical phonons. This proceeding agrees with the numerical work of Refs. 11 and 12 in which the current-voltage characteristic of short nanotubes with lengths smaller than 1  $\mu\text{m}$  is calculated. In contrast to this, Sundqvist *et al.*<sup>13</sup> have in their calculation  $\tau_{\text{ep}}$  values which are around three times smaller than the experimental values. They determine the current-voltage characteristic of nanotubes larger than 1  $\mu\text{m}$  using the one-valley approximation for the electrons. This implies that the electrons are scattered only by one type of phonons, i.e., zone-center phonons,

between the bands within this valley. By using the experimentally determined thermal phonon relaxation lifetime of  $\tau_{\text{op}} \approx 1.1 \pm 0.2$  ps,<sup>18,19</sup> we reach a good agreement with the experimentally determined current-voltage characteristics of large nanotubes. This is in contrast with what happens in short nanotubes, which one has to use at least a five times larger thermal phonon relaxation time to find a reasonable agreement with experiment.

Due to the low dimensionality of a carbon nanotube system in which a fast initial decay of optical phonons is followed by a slow decay of only a small amount of secondary acoustic phonons,<sup>20</sup> we expect a bottleneck in the relaxation path for the hot optical phonons generated by charge-carrier scattering. This idea was used in Ref. 20 to explain the large discrepancy between the radial breathing mode lifetimes measured by Raman-scattering experiments, and by tunneling experiments. Such a bottleneck leads of course to larger effective thermal relaxation times for the optical phonons. In Sec. III we shall describe this fact effectively by taking into account in the phonon Boltzmann description the secondary acoustic phonons in a simple model. By using suitable secondary phonon relaxation times, we were able to reproduce the experimentally determined current-voltage curve also for short tubes. Our result shows that for long tubes the system does not exhibit a phonon bottleneck, in contrast to short nanotubes. We explain this by the fact that at tube length smaller than 1  $\mu\text{m}$ , the thermal scattering lengths of many acoustic phonons reaches the systems size which then dynamically closes relaxation paths for the optical phonons.

We find a similar effect in the interaction of phonons with the electron system under bias voltage. It was shown in Refs. 11 and 12 for short nanotubes that one finds a large increase in the phonon distribution function at the boundaries of the tube. We observe an even worse situation, that we do not find any numerical solution for the Boltzmann equation when setting the optical phonon velocities to zero. In contrast to this, we see for long tubes a phonon distribution function which is peaked in the center of the nanotube, in agreement with experiments for large suspended tubes.<sup>21</sup> In order to understand this effect better, we solve in Sec. IV the system of Boltz-

mann equations for the charge carriers and the phonons analytically within certain approximations. We succeeded in reproducing especially well the large-voltage small-length regime of the numerical determined current-voltage curves. Our calculation shows that the reason for the increase in the temperature at the boundary of tube is again based on the fact that using the phonon relaxation path for small tubes, the electron phonon coupling part in the phonon Boltzmann equation creates effectively an additional phonon relaxation term with a negative sign. This leads to the increase in the phonon temperatures at the boundaries of small tubes.

In the analytical calculations of Sec. IV we determine the electron distribution function under high bias voltages. The appearance of this distribution function is of course much different from the Fermi distribution function in thermodynamical equilibrium. The knowledge of this function opens up a number of possible applications. For example, in Sec. V, we calculate the level broadening and frequency shift of the zone-center optical phonons mediated by the electron-phonon interaction under high bias voltage. We find a positive frequency offset on the zero-bias shift for very large bias voltages, in contrast to the frequency shift mediated by the phonon-phonon scattering with phonons in thermal equilibrium. For very large nanotubes we obtain also a negative frequency offset due to the electron-phonon interaction. The electron-phonon mediated zero-bias broadening of the zone-center optical mode vanishes at high voltages. The results for very high voltages are in agreement with a recent experiment measuring the influence of the high bias on the phonon modes of carbon nanotubes lying on a substrate.<sup>6</sup>

Summarizing, in Sec. II we discuss the results of the coupled electron-phonon Boltzmann system in the relaxation-time approximation numerically. In Sec. III the secondary acoustic phonons in the Boltzmann equation are taken into account. We shall carry out in Sec. IV an analytical calculation of the current-voltage characteristic, the electron and the phonon distribution functions. These functions are used in Sec. V to calculate the level broadening and frequency shift of the optical zone-center phonons mediated by the electron-phonon interaction under high bias voltage.

## II. CURRENT-VOLTAGE CHARACTERISTICS OF CARBON NANOTUBES

The method we use here to calculate the current-voltage characteristic of metallic nanotubes is based on the semiclassical Boltzmann equation. Within this method quantum interference corrections to the conductivity are not taken into account.<sup>22</sup> It was shown just recently through numerical calculations that these corrections to the conductivity are negligible above room temperature for single-walled carbon nanotubes without structural defects due to phonon scattering decoherence mechanisms.<sup>23</sup> Other works using the semiclassical Boltzmann equation for electron or phonon transport not mentioned yet are found in Refs. 24 and 25.

The energy levels of electrons in a nanotube consists of one-dimensional bands positioned in the graphene Brillouin zone around the  $\mathbf{K}$  and  $\mathbf{K}'$  points. For metallic nanotubes two energy bands corresponding to right (R) and left (L)

moving electrons cross at these points. In the following, we assume here that the diameter  $D$  of the nanotube and the applied bias voltage  $U$  is so small that we can neglect electron excitations to higher bands. For example, this is valid for a nanotube with diameter  $D \approx 2$  nm when we apply a bias voltage of less similar to  $U \lesssim 2$  V. The electron distribution functions for a nanotube under bias voltage around the  $\mathbf{K}$  and  $\mathbf{K}'$  points are equal which we denote by  $f_{L/R}(k, x, t)$ . At larger voltages only the optical phonons are relevant as a source of electron-hopping between the bands. The hopping between one band at  $\mathbf{K}$  and the other at the  $\mathbf{K}'$  point are mediated by zone-boundary optical phonons where only Kekulé type of lattice distortions couple to the electronic system.<sup>26</sup> We denote in the following the corresponding phonon distribution function by  $n^K(k, x, t)$ . The hopping between bands at the same  $\mathbf{K}$  or  $\mathbf{K}'$  points are mediated by longitudinal zone-center optical phonons with phonon distribution  $n^\Gamma(k, x, t)$ .<sup>10</sup> The time evolution of the electrons are governed by the semiclassical Boltzmann equation

$$\left( \partial_t + v_F \partial_x + \frac{eE}{\hbar} \partial_k \right) f_{L/R} = [\partial_t f_{L/R}]_c, \quad (1)$$

where the collision term  $[\partial_t f_{L/R}]_c \approx [\partial_t f_{L/R}]_e + [\partial_t f_{L/R}]_{fs} + [\partial_t f_{L/R}]_{bs}$  consists of an elastic scattering term  $[\partial_t f_{L/R}]_e = v_F/l_e [f_R(k) - f_L(k)]$  due to acoustic-phonon scattering (in the quasielastic limit) and impurity scattering.  $l_e$  is the elastic scattering mean-free path. We assume here  $l_e = 1600$  nm.<sup>3,11</sup> The electron velocity  $v_F$  is given by  $v_F = 8.4 \times 10^7$  cm/s and  $e(e > 0)$  is the electronic charge.

$[\partial_t f_{L/R}]_{fs}$  is a forward scattering term which should have a minor effect especially for higher applied voltages since it does not change the propagation direction. The time evolution of optical phonons is given by

$$[\partial_t + v_{op}^\nu(k) \partial_x] n^\nu = [\partial_t n^\nu]_c + [\partial_t n^\nu]_{osc}, \quad (2)$$

where  $\nu = \Gamma, K$  denotes zone-center or zone-boundary phonons. We use here  $v_{op}^\Gamma = \text{sgn}(k) 2.9 \times 10^5$  cm/s and  $v_{op}^K = \text{sgn}(k) 7.2 \times 10^5$  cm/s.<sup>11,17</sup> The term  $[\partial_t n^\nu]_c$  is due to phonon-electron scattering while the term  $[\partial_t n^\nu]_{osc}$  represents thermal phonon relaxation. Note that the coupled electron-phonon system is not heated up by applying large voltages on the nanotube due to this term, which accounts effectively for the scattering of optical phonons into underlying (acoustical) phonons.

Scattering of phonons with electrons leads to two scattering contributions in the electronic Boltzmann Eq. (1) as well as in the phononic Boltzmann Eq. (2). When restricting on the backward scattering contributions we obtain for the electronic scattering term

$$\begin{aligned} [\partial_t f_L]_{bs} = & \sum_\nu \frac{1}{\tau_{ep}^\nu} \{ [n^\nu(k^+, x) + 1] f_R[k_R(\epsilon^+)] \{ 1 - f_L[k_L(\epsilon)] \} \\ & - n^\nu(k^+, x) \{ 1 - f_R[k_R(\epsilon^+)] \} f_L[k_L(\epsilon)] \\ & + n^\nu(-k^-, x) f_R[k_R(\epsilon^-)] \{ 1 - f_L[k_L(\epsilon)] \} \\ & - [1 + n^\nu(-k^-, x)] \{ 1 - f_R[k_R(\epsilon^-)] \} f_L[k_L(\epsilon)] \} \end{aligned} \quad (3)$$

with  $k^\pm = k_R(\epsilon^\pm) - k_L(\epsilon)$  and  $\epsilon^\pm = \epsilon \pm \hbar\omega^\nu$ . The corresponding phononic scattering term results in

$$[\partial_t n^\nu]_c = \sum_\nu \frac{s^\nu}{\tau_{ep}^\nu} ([n^\nu(k, x) + 1] \{f_R(k_R^+) [1 - f_L(k_L^-)] + f_L(-k_L^-) [1 - f_R(-k_R^+)]\} - n^\nu(k, x) \times \{f_L(k_L^-) [1 - f_R(k_R^+)] + f_R(-k_R^+) [1 - f_L(-k_L^-)]\}), \quad (4)$$

where  $k_{R/L}^\pm = k_{R/L}(\epsilon(k/2) \pm \hbar\omega^\nu/2)$ . The number  $s^\nu$  is given by  $s^K=1$  for zone-boundary phonons and  $s^\Gamma=2$  for zone-center ones.<sup>11</sup> In order to derive these numbers one has to take into account that momentum phase space of the phonons is twice as large as the phase space of the electrons. Further one has to consider the fact that the electron jumps from the  $\mathbf{K}$  to the  $\mathbf{K}'$  band are mediated by  $\mathbf{K}$  phonons but the reverse jumps by  $\mathbf{K}'$  phonons. On the other hand jumps of electrons within the same valley are mediated by the same  $\Gamma$  phonons. Finally, we mention here that we used the boundary conditions<sup>11</sup>

$$f_L[k_L(\epsilon), L] = f_R[k_R(\epsilon), 0] = n_F(\epsilon), \quad (5)$$

$$n^\nu(k > 0, 0) = n^\nu(k < 0, L) = n_B^{\text{op}}, \quad (6)$$

where  $n_F(\epsilon)$  is the Fermi function for a metallic nanotube with zero gate voltage at room temperature, i.e.,  $n_F(\epsilon) = 1/(1 + e^{\epsilon/k_B T})$ , and  $n_B^{\text{op}}$  is the Boltzmann factor for optical phonons at room temperature given by  $n_B^{\text{op}} \approx 0.0014$ . We use optical phonon frequencies  $\hbar\omega^K = 161$  meV and  $\hbar\omega^\Gamma = 196$  meV. The electron-phonon scattering times for zone-center and zone-boundary optical phonons are given by  $\tau_{ep}^\Gamma = 538$  fs and  $\tau_{ep}^K = 219$  fs (Ref. 10) where we assume tube diameters of around 2.0 nm typical in existing current-voltage experiments in the literature.

Our method to solve Eqs. (1) and (2) is based on the numerical time integration by the standard splitting method.<sup>27</sup> We discretize the differential equations in momentum and position space.<sup>28</sup> To integrate the collisionless free electron and phonon equations in some time step, we use the exact solution of the equations in the case of the electron motion. This means that the time step values are fixed by the space grid. The free phonon motion in one time step is given by the up integration of the collisionless discrete version of Eq. (2) on the space grid.

In this section, we use a standard single-mode relaxation-time approximation for the optical phonon scattering term  $[\partial_t n^\nu]_{\text{osc}}$  given by

$$[\partial_t n^\nu]_{\text{osc}} = -\frac{1}{\tau_{\text{op}}} (n^\nu - n_B^{\text{op}}). \quad (7)$$

Note that this approximation is only valid for the system lying on a substrate. For the suspended nanotube system one has to take into account explicitly the heat transfer by acoustic phonons to the leads.<sup>5</sup> We assume in our calculation that the thermal relaxation time  $\tau_{\text{op}}$  is similar for zone-center and zone-boundary optical phonons. This approximation is justified for graphene in Ref. 29 where it is shown that the relax-

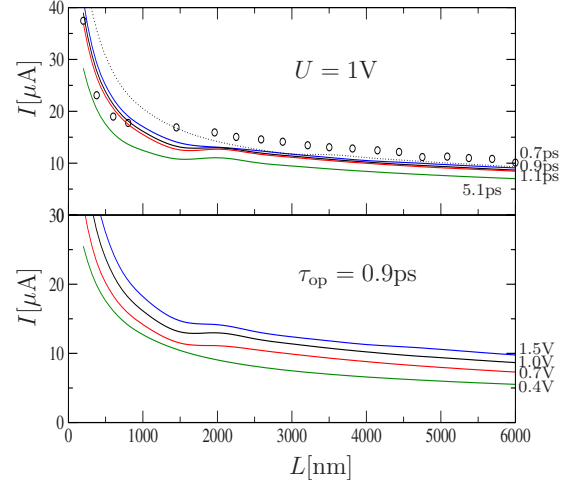


FIG. 1. (Color online) Upper panel shows the current-voltage characteristic of long nanotubes with diameter  $D=2.0$  nm for bias voltage  $U=1$  V calculated by the help of Eqs. (1)–(7) for various thermal relaxation times  $\tau_{\text{op}}$  (solid curves) and  $l_e=1600$  nm. The dotted curve shows the current-voltage characteristic of a  $D=2.8$  nm nanotube, i.e., it uses  $\sqrt{2}\tau_{ep}^\nu$  as the electron-phonon scattering times, and  $\tau_{\text{op}}=0.9$  ps. The (black) circles are given by the experiment (Ref. 8). The lower panel shows the current-voltage characteristic of long nanotubes with diameter  $D=2.0$  nm for various bias voltages,  $\tau_{\text{op}}=0.9$  ps and  $l_e=1600$  nm.

ation times of both phonon types are almost equal for acoustic phonon temperatures a little higher than the room temperature. We do not expect a difference for carbon nanotubes. These temperatures are immediately reached at the high-voltage experiments we are interested in.<sup>6,7,9,21</sup>

First we calculate the current-voltage characteristic for nanotubes of length larger than 1  $\mu\text{m}$  in the vicinity of  $\tau_{\text{op}}=1.1$  ps. This value is chosen since Song *et al.*<sup>18</sup> determined experimentally  $\tau_{\text{op}}=1.1 \pm 0.2$  ps in agreement to the experiment of Kang *et al.* in Ref. 19.

In the upper panel in Fig. 1 the current-voltage characteristic determined with help of Eqs. (1)–(7) is shown for nanotubes at bias voltage  $U=EL=1$  V as a function of their length for various relaxation times  $\tau_{\text{op}}$  in the vicinity of the experimentally determined relaxation time. The solid curve in the figure is given by the experiment carried out by Sundqvist *et al.* in Ref. 8. In this experiment the nanotube length was effectively varied by changing the distance between the electrodes where the bias voltage is applied.

We get the best agreement within the experimental uncertainties for the quantity  $\tau_{\text{op}}=1.1 \pm 0.2$  ps at value  $\tau_{\text{op}}=0.9$  ps. In the lower panel in Fig. 1, we calculate the current-voltage characteristic of nanotubes for  $\tau_{\text{op}}=0.9$  ps as a function of the tube length for various bias voltages. Figure 2 shows the average phonon density for a nanotube at length  $L=3000$  nm,  $U=1$  V and  $\tau_{\text{op}}=0.9$ . This density is determined by

$$\bar{n}^\nu(x) = \frac{1}{2eEL} \int_{eE(x-L)}^{eEx} d\epsilon \{n^\nu[2k_L(\epsilon), x] + n^\nu[2k_R(\epsilon), x]\}. \quad (8)$$

The factor 2 in the denominator is necessary due to the fact that we average over the right- and left-moving electron

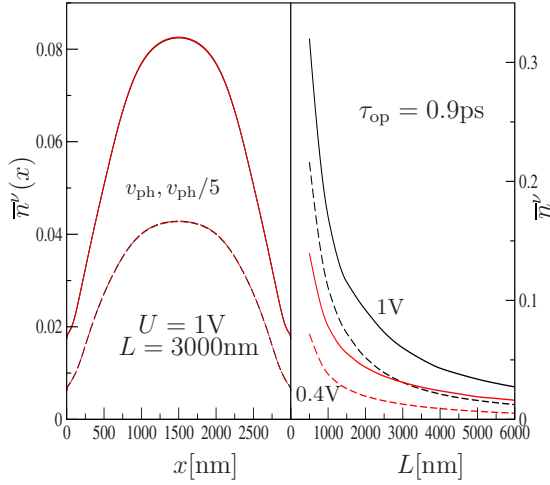


FIG. 2. (Color online) Left panel shows the phonon-density distribution functions  $\bar{n}^K(x)$  (solid curves) and  $\bar{n}^\Gamma(x)$  (dashed curves) defined in Eq. (8) for  $U=1$  V,  $\tau_{op}=0.9$  ps and  $L=3000$  nm. The black curve is calculated by using the former defined  $v_{op}^\Gamma = \text{sgn}(k)2.9 \times 10^5$  cm/s and  $v_{pp}^K = \text{sgn}(k)7.2 \times 10^5$  cm/s (Refs. 11 and 17). The red curves uses  $v_{op}^\Gamma/5$  and  $v_{pp}^K/5$  as phonon velocities. The curves lie practical on top of each other. The right panel shows position-averaged phonon distribution functions  $\bar{n}^K$  (solid curves) and  $\bar{n}^\Gamma$  (dashed curves) for  $U=0.4$  V (lower red curves) and  $U=1$  V (upper black curves) for  $\tau_{op}=0.9$  ps.

bands. We obtain phonon densities which are peaked in the center of the nanotubes. This behavior is in accordance to experiments<sup>21</sup> for suspended nanotubes. We show also in this figure the space averaged phonon densities  $\bar{n}^\nu = \int dx \bar{n}^\nu(x)/L$  as a function of the tube length for various bias voltages.

One reason for the small difference in the current-voltage characteristic between experiment and theory in the upper panel of Fig. 1 at large nanotube lengths is due to the fact that the diameter  $D$  of the tube in the experiment Ref. 8 is in fact a little larger than 2 nm. Although the diameter was not measured explicitly in Ref. 8 one can estimate it by the fact that Sundqvist *et al.* measured approximately half of the differential resistivity for short distances between the electrodes in comparison to the value in Refs. 3 and 4. In these experiments the current-voltage characteristic of short nanotubes with a measured diameter  $D \approx 2$  nm was recorded. By using an analytical theory for the current-voltage characteristic which will be derived in Sec. IV and further that the electron-phonon scattering time  $\tau_{ep}^\nu$  is proportional to the diameter  $D$  of the nanotube<sup>10</sup> we obtain that  $D \approx \sqrt{2} \times 2$  nm  $\approx 2.8$  nm. We show in the upper panel in Fig. 1 by the dotted curve the theoretically calculated current-voltage characteristic for a 2.8 nm nanotube, i.e.,  $\tau_{ep}^\nu$  is now a factor  $\sqrt{2}$  larger than for the 2.0 nm nanotube already used before, and  $\tau_{op}=0.9$  ps.

In contrast to the small undershooting of the theoretically determined current-voltage curve in comparison to the experimental curve for large lengths in Fig. 1, we obtain for small nanotube lengths an overshooting of the curve. The reason for this different behavior between large and small nanotube lengths will be discussed in the following.

Next, we determine the current-voltage characteristic of short nanotubes. In Fig. 3 we show the current-voltage char-

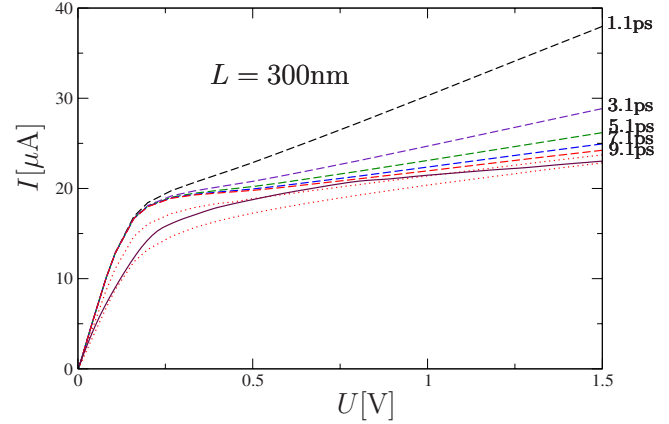


FIG. 3. (Color online) Current-voltage characteristic of a  $L=300$  nm nanotube calculated by the help of Eqs. (1)–(7) for various thermal relaxation times  $\tau_{op}$  (dashed curves) and  $l_e=1600$  nm. The (black) solid curve is given by the experiment (Ref. 4). The (red) dotted curves are calculated for  $\tau_{op}=9.1$  ps,  $l_e=800$  nm (upper curve), and  $l_e=400$  nm (lower curve).

acteristic for a nanotube of length  $L=300$  nm as a function of the bias voltage  $U$  for various phonon relaxation times  $\tau_{op}$ . The solid curve is given by the experiment.<sup>4</sup> We obtain the best agreement between experiment and theory for the differential conductivity  $dU/dI \approx 220$  k $\Omega$  at  $\tau_{op} \approx 9.1$  ps. It is astonishing that this optical phonon relaxation time is much larger than the experimentally determined optical phonon relaxation time  $\tau_{op}=1.1 \pm 0.2$  ps. The reason for this discrepancy will be discussed in the next section. Note that we obtain in Fig. 3 in the low-voltage regime a better agreement between the theoretically and experimentally determined curves by using smaller elastic scattering lengths  $l_e < 1600$  nm.

### III. SECOND-GENERATION PHONONS

From Fig. 3 we see that a satisfactory agreement between the experimentally and numerically determined current-voltage characteristic is only reached for  $\tau_{op} \gg 1.1$  ps. On the other hand, recent phonon lifetime experiments on carbon nanotubes show that  $\tau_{op} \approx 1.1$  ps for zone-center phonons.<sup>18,19</sup> These measured phonon lifetimes are governed by the decay of zone-center phonons to two lower energetic second-generation phonons where the number of these decay channels should be rather small for one-dimensional nanotube systems in contrast to higher dimensional systems such as graphene or graphite.<sup>20</sup> The second-generation phonons are typically acoustic ones which then again scatter in two acoustic phonons with even lower energy and longer wavelength where this lifetime is much longer than of the primary optical phonons. The reason for the longer lifetime comes from the fact that the three phonon matrix element vanishes in the long-wavelength limit and further that the phase space for phonon decay is smaller for lower phonon energies due to energy conservation. The long lifetime of secondary phonons and the small amount of possible decay channels could lead to a bottleneck in the decay process. This means that a sig-

nificant amount of secondary phonons are assembled in the decay of hot phonons generated by charge carriers through the electron-phonon interaction. When this nonequilibrium amount of secondary phonons is similar to the number of equilibrium phonons following the Bose-Einstein distribution the single-mode relaxation time method leading to the appearance of the scattering expression (7) is no longer valid. In Ref. 20 it was argued that this fact is responsible for the considerable difference in the lifetime measurements of the radial breathing mode by using either Raman-scattering experiments or electron tunnel experiments. The decay channel can then be described by the following Boltzmann equations<sup>30</sup> when neglecting the phonon velocities  $v_{\text{op}}^v \approx 0$  on the left-hand side of Eq. (2),

$$\partial_t n^v = \frac{1}{\tau_{\text{op}}} [-n^v(1+n_{\text{ac}})^2 + (1+n^v)n_{\text{ac}}^2] + [\partial_t n^v]_c, \quad (9)$$

$$\partial_t n_{\text{ac}} = \frac{1}{p\tau_{\text{op}}} [n^v(1+n_{\text{ac}})^2 - (1+n^v)n_{\text{ac}}^2] - \frac{1}{\tau_{\text{ac}}} (n_{\text{ac}} - n_B^{\text{ac}}). \quad (10)$$

Here the first term in the brackets in Eq. (9) describes the scattering of the optical phonons with distribution function  $n^v$  into two secondary phonons with distribution function  $n_{\text{ac}}$ . For simplicity we assumed that the secondary phonons follow all the same distribution function.

The second term in the brackets in Eq. (9) describes the reverse process. The second Eq. (10) describes the dynamics of the secondary phonons. Here  $p$  denotes the number of decay channels. For one-dimensional solids this number is generally small.<sup>20</sup> For simplicity we further assumed in Eq. (10) that the secondary phonons are coupled to a heat bath where the relaxation with this bath happens in time  $\tau_{\text{ac}} \gg \tau_{\text{op}}$ . The quantity  $n_B^{\text{ac}}$  is the Bose factor for the secondary phonons which we assume to be half of the frequency of the optical primary phonons, leading to  $n_B^{\text{ac}} \approx 0.03$  at room temperature. Note that this choice is consistent with the fact that we choose uniform secondary phonon distributions.

In the stationary case we have  $\partial_t n_{\text{ac}} = 0$ . Then we can solve the second Eq. (10) for  $n_{\text{ac}}$  and insert the result into the first equation which leads to an effective optical phonon scattering term

$$[\partial_t n^v]_{\text{osc}} = -\frac{1}{\tau_{\text{op}}} \left[ (n^v - n_B^{\text{ac}}) \frac{p\tau_{\text{op}}}{\tau_{\text{ac}}} - \frac{1}{2} \left( \frac{p\tau_{\text{op}}}{\tau_{\text{ac}}} \right)^2 + \frac{1}{2} \frac{p\tau_{\text{op}}}{\tau_{\text{ac}}} \sqrt{\left( \frac{p\tau_{\text{op}}}{\tau_{\text{ac}}} - 2n^v \right)^2 + 4 \left( n^v + \frac{p\tau_{\text{op}}}{\tau_{\text{ac}}} n_B^{\text{ac}} \right)} \right] \quad (11)$$

with limits

$$\lim_{p\tau_{\text{op}}/\tau_{\text{ac}} \rightarrow \infty} [\partial_t n^v]_{\text{osc}} \rightarrow -\frac{1}{\tau_{\text{op}}} [n^v(1+2n_B^{\text{ac}}) - (n_B^{\text{ac}})^2], \quad (12)$$

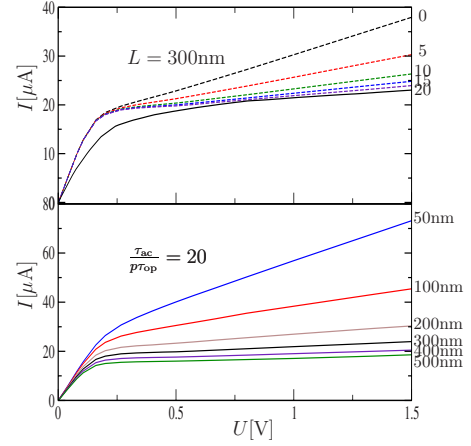


FIG. 4. (Color online) Upper panel shows the current-voltage characteristic of a  $L=300$  nm nanotube calculated by the help of Eqs. (1)–(4) and (11) for various parameters  $\tau_{\text{ac}}/p\tau_{\text{op}}$  (dashed curves) and  $\tau_{\text{op}}=1.1$  ps,  $l_e=1600$  nm. The (black) solid curve is given by the experiment (Ref. 4). The lower panel shows the current-voltage characteristic of various nanotubes with different lengths for  $\tau_{\text{op}}=1.1$  ps and  $\tau_{\text{ac}}/p\tau_{\text{op}}=20$ ,  $l_e=1600$  nm.

$$\lim_{p\tau_{\text{op}}/\tau_{\text{ac}} \rightarrow 0} [\partial_t n^v]_{\text{osc}} \rightarrow -\frac{1}{\tau_{\text{op}}} \frac{p\tau_{\text{op}}}{\tau_{\text{ac}}} \left[ \left( 1 + \sqrt{1 + \frac{1}{n^v}} \right) n^v - n_B^{\text{ac}} \right]. \quad (13)$$

As is seen from Eq. (12) in the case of no existent bottleneck, i.e., large  $p\tau_{\text{op}}/\tau_{\text{ac}}$  and small Boltzmann factors  $n_B^{\text{op}}$ ,  $n_B^{\text{ac}}$  valid in our case, we obtain the standard single-mode relaxation-time approximation (7) for the optical phonon scattering term.

In the following, we carry out the numerical calculation by using Eqs. (1)–(4) with the optical phonon scattering term (11) substituting Eq. (7). From Eq. (11) we obtain that the optical scattering term depends via  $\tau_{\text{ac}}/p\tau_{\text{op}}$  on the acoustic scattering length. We show in the upper panel of Fig. 4 the current voltage characteristic for various parameters  $\tau_{\text{ac}}/p\tau_{\text{op}}$ ,  $\tau_{\text{op}}=1.1$  ps and nanotubes of length  $L \approx 300$  nm. This figure should be compared to Fig. 3 in the case of the single-mode relaxation time approximation which uses Eq. (7) for the optical phonon scattering term. We obtain a similar behavior of the current-voltage characteristic curves in both approximations. The reason is seen from expression (13). We obtain from this expression and the fact that at room temperature  $n_B^{\text{ac}}$ ,  $n_B^{\text{op}} \ll 1$  as well as  $n^v \gg 1$  for high bias voltages, that for small  $p\tau_{\text{op}}/\tau_{\text{ac}}$  the effective optical phonon scattering term  $[\partial_t n^v]_{\text{osc}}$  has still the standard single-mode relaxation term (7). The effective relaxation time  $\tau_{\text{op}}$  is then changed to  $\tau_{\text{op}} \rightarrow \tau_{\text{ac}}/2p$  which respects the fact that the relaxation of the optical phonons are effectively relaxed on  $2p$  channels of relaxation time  $\tau_{\text{ac}}$ .

In the lower panel of Fig. 4 we show the current-voltage characteristic for various nanotube lengths by using Eq. (11) as the optical phonon scattering term with  $\tau_{\text{ac}}/p\tau_{\text{op}}=20$  and  $\tau_{\text{op}}=1.1$  ps. Figure 5 shows the energy-averaged phonon distribution function (8)  $\bar{n}^v(x)$  (left panel) and the energy and position-averaged phonon distribution function  $\bar{n}^v$  (right

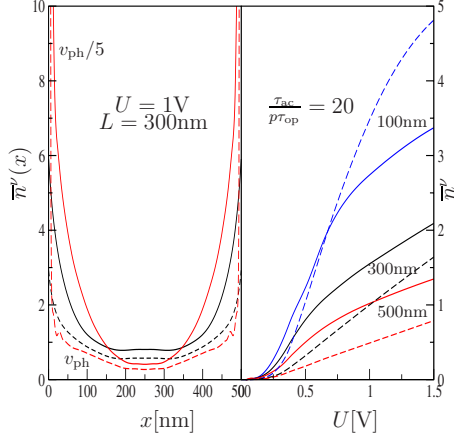


FIG. 5. (Color online) Left panel shows the phonon-density distribution functions  $\bar{n}^K(x)$  (solid curves) and  $\bar{n}^I(x)$  (dashed curves) defined in Eq. (8) for  $U=1$  V and  $\tau_{ac}/p\tau_{op}=20$ ,  $\tau_{op}=1.1$  ps, and  $L=300$  nm. The black curve is calculated by using the former defined phonon velocities  $v_{op}^\Gamma = \text{sgn}(k)2.9 \times 10^5$  cm/s and  $v_{op}^K = \text{sgn}(k)7.2 \times 10^5$  cm/s (Refs. 11 and 17). The upper (red) curves use  $v_{op}^\Gamma/5$  and  $v_{op}^K/5$  as phonon velocities. The right panel shows position-averaged phonon distribution functions  $\bar{n}^I$  (dashed curves) and  $\bar{n}^K$  (solid curves) for  $U=1$  V,  $\tau_{ac}/p\tau_{op}=20$  and  $L=100$  nm (blue curves), 300 nm (black curves) and 500 nm (red curves).

panel) for various nanotube lengths. We obtain that in contrast to the case of large nanotubes in Fig. 2, the short nanotubes show an increasing phonon density at the boundary of the nanotube.<sup>11,12</sup> We obtain from the left panel in Fig. 5 the even worse fact of a diverging current-voltage characteristic for phonon velocities  $v_{op}^v \rightarrow 0$ . We shall understand this unusual behavior better in the next section where we show an analytic solution of the Boltzmann system [Eqs. (1)–(7)].

Summarizing, by taking into account a possible bottleneck in the optical phonon relaxation path we obtain for an optical phonon relaxation time  $\tau_{op}=1.1$  ps for large nanotubes an effective scattering parameter  $\tau_{ac}/p\tau_{op}=0$  as the best-fitting parameter to the experimental curves, i.e., no phonon bottleneck is seen in this case. On the other hand for small nanotubes and  $\tau_{op}=1.1$  ps we obtain an effective scattering parameter of  $\tau_{ac}/p\tau_{op}=20$ . The reason for this discrepancy between large and small nanotubes lies in the fact that we have neglected the velocities of the secondary phonons in the Boltzmann Eq. (10). This leads in the case of the decay of zone-center optical phonons to additional terms of the form  $\pm v_{ac}\partial_x n_{ac}^\pm$  in the left hand side of Eq. (10) where  $n_{ac}^\pm$  stands for the left- and right-moving phonon in a scattering pair. This means that we remove the restriction in the right-hand sides of Eqs. (9) and (10) that the scattering pairs have all the same distribution function. To see when the  $\pm v_{ac}\partial_x n_{ac}^\pm$  term becomes relevant in the Boltzmann equation we further have to take into account the number of decay channels  $p$  for nanotubes. In the following we restrict ourselves to the relaxation of the zone-center phonons. The argument for the zone-boundary phonons works similar.

It was shown in Refs. 20 and 29 that in the case of graphene the zone-center optical phonons scatter into three sorts of different pairs of phonons lying on rings in the Brillouin zone around the  $\Gamma$  points where scattering into the

longitudinal acoustic sector is in fact the most dominant. In order to estimate from this fact the number of pairs for a nanotube with diameter of around 2 nm we use in the following the zone-folding approximation method. By using as an approximation that in the case of graphene the decay rings lie in the mids between the  $\Gamma$  and  $\mathbf{K}$  point (best fulfilled for the longitudinal mode<sup>20,29</sup>) we obtain as an estimate for the number of decay pairs  $p \lesssim 20$  in a 2 nm nanotube. In order to see no bottleneck in the relaxation process for large nanotubes we have  $\tau_{ac} \lesssim p\tau_{op}$  meaning that  $\tau_{ac} \lesssim 22$  ps. On the other hand for a nanotube of diameter 2 nm one obtains for the lowest lying phonon modes in a simple model relaxation times which are larger than around  $\tau_{ac} \gtrsim 20$  ps.<sup>31</sup> This leads us to the estimate  $\tau_{ac} \sim 20$  ps for the effective acoustic relaxation time. With  $v_{ac} \sim 21$  km/s (we choose the maximum velocity value for acoustic phonons in graphite<sup>32–34</sup>) we obtain that the acoustic phonon velocity terms  $\pm v_{ac}\partial_x n_{ac}^\pm \sim \pm v_{ac}n_{ac}^\pm/L$  in the phonon Boltzmann equation becomes relevant for  $L \lesssim 420$  nm. This is only a very rough approximation for this length.

At this length we find that for one participant of the scattered acoustic phonon pairs this additional relaxation term is not relevant since the relaxation path is already open. For the other participant this term leads to a closing of the relaxation path which we saw in our numerics as an increase in the effective relaxation parameter  $\tau_{ac}/p\tau_{op}$ .

#### IV. ANALYTIC CALCULATION

Due to the similarity of the phonon frequency of zone-boundary phonons  $\omega^K$  and zone-center phonons  $\omega^\Gamma$  and since the electron-phonon coupling constants  $s^K/\tau_{ep}^K$  and  $s^\Gamma/\tau_{ep}^\Gamma$  are similar we use in the following the simplification that the nanotube system interacts with only one sort of phonons with frequencies  $\omega$ . The effective electron-phonon scattering parameter  $\tau_{ep}$  in the electronic sector, the electron-phonon scattering parameter  $s^p/\tau_{ep}$  in the phononic sector and phonon velocities  $v_{ph}$  are chosen in the following way:

$$\begin{aligned} \hbar\omega &= \hbar \left( \frac{\omega^K}{\tau_{ep}^K} + \frac{\omega^\Gamma}{\tau_{ep}^\Gamma} \right) / \left( \frac{1}{\tau_{ep}^K} + \frac{1}{\tau_{ep}^\Gamma} \right) = 170 \text{ meV}, \\ \frac{1}{\tau_{ep}} &= \left( \frac{1}{\tau_{ep}^K} + \frac{1}{\tau_{ep}^\Gamma} \right) = \frac{1}{155 \text{ fs}}, \\ \frac{s^p}{\tau_{ep}} &= \left( \frac{s^K}{(\tau_{ep}^K)^2} + \frac{s^\Gamma}{(\tau_{ep}^\Gamma)^2} \right) / \left( \frac{1}{\tau_{ep}^K} + \frac{1}{\tau_{ep}^\Gamma} \right) = \frac{1}{231 \text{ fs}}, \\ v_{ph} &= \frac{v_{ph}^K}{\tau_{ep}^K} + \frac{v_{ph}^\Gamma}{\tau_{ep}^\Gamma} / \left( \frac{1}{\tau_{ep}^K} + \frac{1}{\tau_{ep}^\Gamma} \right) = \text{sgn}(k)5.95 \times 10^5 \frac{\text{cm}}{\text{s}}. \end{aligned} \quad (14)$$

In the following discussion, we use the abbreviation  $l'_{sc} \equiv v_F\tau_{ep}/(2\bar{n}+1)$  for the reduced effective scattering length and  $l_{sc} \equiv L/(1+L/l'_{sc})$  for the total scattering length.

Below, we solve the Boltzmann Eqs. (1) and (2) for large voltages  $eU \gg \hbar\omega$  and lengths  $L \gg l'_{sc}$  analytically by the help

of two approximations. In the first approximation we use in the electronic Boltzmann Eq. (1) positional and momentum-independent phonon distribution functions  $n(k, x) \approx \bar{n}$ . We shall determine  $\bar{n}$  then similarly to Eq. (8) where the energy average is taken over those energies where  $n(k, x)$  or  $f_L(k, x)$ ,  $f_R(k, x)$  are nonzero, respectively. Thus we neglect large (infinite) energy regions where the electron and phonon distribution functions are zero since they do not contribute to the current.

In the calculation below, we find for the energy-averaged phonon distribution functions

$$\bar{n}(x) = \frac{1}{2(\epsilon_u - \epsilon_d)} \int_{\epsilon_d}^{\epsilon_u} d\epsilon n(2k_L(\epsilon), x) + n(2k_R(\epsilon), x), \quad (15)$$

where

$$\epsilon_u = \begin{cases} eEx & \text{for } \pi \frac{eUl_{sc}}{L} \gg \hbar\omega, \\ \frac{\omega L}{\pi l_{sc}} & \text{for } \pi \frac{eUl_{sc}}{L} \ll \hbar\omega \end{cases} \quad (16)$$

and

$$\epsilon_d = \begin{cases} eE(x-L) & \text{for } \pi \frac{eUl_{sc}}{L} \gg \hbar\omega, \\ 0 & \text{for } \pi \frac{eUl_{sc}}{L} \ll \hbar\omega. \end{cases} \quad (17)$$

$\bar{n}$  is then determined by the average

$$\bar{n} = \frac{1}{L} \int_0^L dx \bar{n}(x). \quad (18)$$

The second approximation is given by a linearization of the nonlinear scattering terms in Eq. (3) which can be identified by extracting the brackets in Eq. (3). These terms are equal to the terms followed by setting in Eq. (3)  $n^\nu$  equal to zero. To linearize these terms we should take care on the expansion points  $\bar{f}_L$  where  $f_L = \bar{f}_L + \Delta f_L$  and similar for  $f_R$ . In a first crude approximation we use in the following as the expansion point  $\bar{f}_L = \bar{f}_R = 1$  which are the boundary values [Eq. (5)] for  $f_L$  and  $f_R$  on the nonzero momentum support of the electronic distribution function. Then we obtain

$$f_R[k_R(\epsilon + \hbar\omega^\nu)] \{1 - f_L[k_L(\epsilon)]\} - f_L[k_L(\epsilon)] \\ \times \{1 - f_R[k_R(\epsilon - \hbar\omega^\nu)]\} \approx f_R[k_R(\epsilon - \hbar\omega^\nu)] - f_L[k_L(\epsilon)]. \quad (19)$$

#### A. Current-voltage characteristic and electron distribution function

With the help of the approximations (18) and (19) one can solve Eq. (1) with Eq. (3) using Fourier methods. After a lengthy calculation carried out in Appendix we obtain for the electron distribution function  $f_L[x, k_L(\epsilon)]$  Eq. (A5) with Eqs. (A6) and (A11). The distribution function  $f_R[x, k_R(\epsilon)]$  is then given by  $f_L[x, k_L(\epsilon)]$  with the help of the substitution (A4).

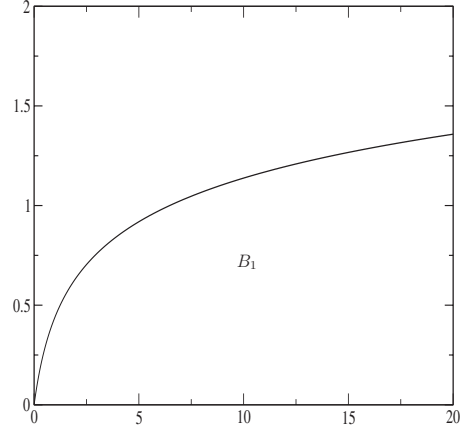


FIG. 6. We show the function  $B_1(x)$  defined in Eq. (A13).

The current-voltage characteristic is given by Eq. (A12)

$$I = 4 \frac{e}{h} \left[ \hbar\omega B_1 \left( \frac{1 + L/l_{sc}^r}{\pi\bar{n}} \right) + \frac{eU}{(1 + L/l_{sc}^r)} \right], \quad (20)$$

where  $B_1(x)$  is defined in Eq. (A13) and plotted in Fig. 6. By taking into account the regime  $\bar{n} \geq 1$ ,  $v_F \tau_{ep} \approx 130$  we obtain for  $L=300$  nm that  $B_1 \approx 0.5$ . By using  $l_{sc} \approx 10.4$  nm (this will be shown below by using Fig. 7) we obtain excellent agreement with the numerically determined current-voltage characteristic at high voltages shown in Fig. 3 and with experiments<sup>3,4</sup> measuring  $l_{sc} \approx 10-11$  nm. Note that the first term in Eq. (20) corresponds to the y-axis value obtained by extending the high-voltage curves to this axis. For this we further note that  $4(e/h)\hbar\omega \approx 26.6$   $\mu$ A.

Next, we discuss the current-voltage characteristic for large lengths, i.e.,  $l_{sc}/L \ll \tau_{ep}/\tau_{op}$  and low voltages  $\pi eU \ll \hbar\omega L/l_{sc}$ . Here, we obtain  $\bar{n} \approx 1.2$  (see the discussion in Sec. IV B 2) leading with Fig. 6 to  $B_1 \approx 1.3$  for nanotube lengths  $L \approx 3000$  nm. This leads to currents which are approximately two times the current values shown in Fig. 1.

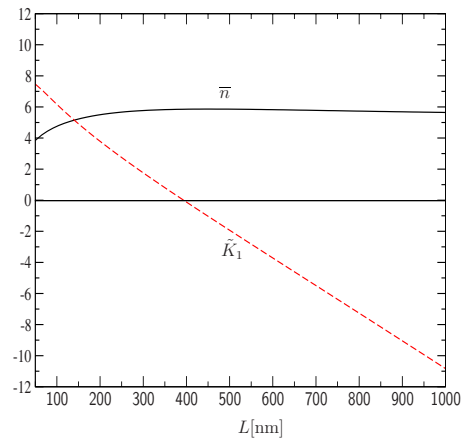


FIG. 7. (Color online) The (black) solid curve is given by the phonon distribution function  $\bar{n}$  as a function of the nanotube length  $L$  calculated with the help of Eq. (A26) with Eqs. (A27)–(A29). The (red) dashed curve shows  $\bar{K}_1$  [Eq. (A21)] as a function the nanotube length  $L$  in the parameter regime  $\mathcal{R}_2$  [Eq. (A17)] using  $\bar{n}$ .

Although this value is too large, the overall behavior of an approximately length independent current for fixed bias voltage shown in the numerical calculation in Fig. 1, is also seen in the analytic calculation.

Summarizing, from Eq. (20) we obtain a different behavior of the current-voltage characteristic in the regime  $\pi eU \gg \hbar\omega L/l_{sc}$  where the second term in Eq. (20) is the leading contribution to the current and the regime  $\pi eU \ll \hbar\omega L/l_{sc}$  where the first term is most relevant. The reason for this can be seen in Eqs. (1) and (3). At low optical phonon scattering rates, i.e.,  $\pi eU \gg \hbar\omega L/l_{sc}$ , electron scattering takes primarily place from the upper part of the filled right-moving band to the empty part of left-moving band. For higher scattering rates  $\pi eU \ll \hbar\omega L/l_{sc}$  a large amount of electrons are also able to be scattered from the upper part of the filled right-moving band to the filled part of the left-moving band within many scattering processes where now Pauli blocking prohibits this scattering. This Pauli blocking is only roughly described by the linearized phonon scattering approximation (19). This is the reason that in the large length regime we obtain less agreement between our numerical and analytical results in contrast to nanotubes of smaller lengths.

### B. Phonon distribution functions

Next, we determine the phonon distribution function  $n(k, x)$  by solving Eq. (2) with Eqs. (4) and (7). We use here in our analytical calculation for simplicity the standard relaxation-time approximation (7) for the optical scattering term instead of the more complicated scattering term (11) which takes into account also the second-generation phonons. As was discussed in Sec. III the differences in the current-voltage characteristic are only minor when taking the effective optical phonon relaxation times  $\tau_{op}=0.9$  ps for long nanotubes and  $\tau_{op}\approx 9.1$  ps for short ones. We shall determine first the phonon distribution function  $n(k, x)$  in the regime  $\pi eU \gg \hbar\omega L/l_{sc}$ .

#### 1. Phonon distribution function for $\pi eU \gg \hbar\omega L/l_{sc}$

We obtain in Appendix for  $n(k, x)$  Eqs. (A18)–(A20) for  $k > 0$  in the different parameter regimes [Eq. (A15)]. For  $k < 0$ ,  $n(k, x)$  is given by  $n(-k, -x)$  Eq. (A14) where the  $K_1$ s are defined in Eq. (A17). From these equations we can calculate the energy-averaged phonon distribution function  $\bar{n}(x)$ . This function is given by Eq. (A22) with Eqs. (A23)–(A25). From this function we obtain for the position-averaged phonon distribution function  $\bar{n}$  Eq. (A26) with Eqs. (A27)–(A29). This function determines effectively the averaged phonon distribution function by using the definition for  $\tilde{K}_1$  [Eq. (A21)] in the regime  $\mathcal{R}_2$  [Eq. (A15)]. We solved this equation analytically below Eq. (A30) in various nanotube length regimes. In Fig. 7 we show the numerical solutions for  $\bar{n}$  and  $\tilde{K}_1$  in the regime  $\mathcal{R}_2$  as a function of the nanotube length  $L$ . For a nanotube of length  $L=300$  nm we obtain  $l_{sc} \approx 10.4$  and  $\tilde{K}_1 \approx 0$ . For these values we obtain Eq. (A31) for  $\bar{n}(x)$  showing in fact a phonon distribution function which increases at the boundary of the nanotube. From Eq. (A25) we obtain that this behavior is even more pronounced for  $\tilde{K}_1$  values larger than zero.

#### 2. Phonon distribution function for $\pi eU \ll \hbar\omega L/l_{sc}$

In the following, we restrict ourselves to the regime where  $l_{sc}/L \ll \tau_{ep}/\tau_{op}$  which is good fulfilled in the large length regime considered in Sec. II. By taking into account Eqs. (A4), (A6), and (A11) we obtain that  $n(k, x) \neq n_B^{ac}$  only in the regime  $|\pi(\hbar v_F |k|/2\omega)L/l_{sc}| \leq 1$  where we take into account that  $\bar{n} \leq 1$  as will be shown immediately below.

This leads to Eq. (A34) for  $n(k, x)$  and Eq. (A35) for  $\bar{n}(x)$ ,  $\bar{n}$  in this regime. By taking into account  $s^p \tau_{op}/\tau_{ep} \approx 4.76$  we obtain  $\bar{n} \approx 1.2$ . Note this value is much larger than the numerical determined values shown in Fig. 2.

### V. ELECTRON-PHONON COUPLING INDUCED FREQUENCY SHIFT AND LIFETIMES OF OPTICAL PHONONS AT HIGH BIAS

By using the electron distribution functions  $f_L$  Eq. (A5) with Eqs. (A6) and (A11) and  $f_R$  Eq. (A4) we are now able to calculate the effect of a large bias voltage on the frequency shift and lifetimes of optical phonons. We restrict our calculation to the Raman-active zone center  $\Gamma$  phonons. In this section, we shall carry out a similar calculation as was done in Ref. 35 for the frequency shift and lifetimes of optical phonons at zero-bias voltage and temperature  $T=0$ . There, the electron distribution functions  $f_L$  and  $f_R$  are Fermi functions. The retarded phonon self-energy at zero momentum is given by

$$\Pi^{L,T}(\omega) = \sum_n \int_{-1/2}^{1/2} dt [\Pi^{L,T}(n, \omega) - \Pi^{L,T}(n+t, 0)], \quad (21)$$

where  $\Pi^{L,T}(n, \omega)$  is the self-energy contribution of the  $n$ th electron band. Its value is given by<sup>35</sup>

$$\begin{aligned} \Pi^{L,T}(n, \omega) = & -4 \sum_{s,s'} \sum_k dt \left( \frac{\beta\gamma}{b^2} \right)^2 \frac{\hbar}{NM\omega^\Gamma} \\ & \times \frac{1}{2} \left( 1 \pm \frac{ss'[\kappa^2[n] - k^2]}{\kappa^2[n] + k^2} \right) \\ & \times \frac{f[\epsilon^s(n, k)] - f[\epsilon^{s'}(n, k)]}{\hbar\omega - \epsilon^s(n, k) + \epsilon^{s'}(n, k) + i0}, \quad (22) \end{aligned}$$

where the electron bands for metallic nanotubes are given by

$$\epsilon^s(n, k) = s\hbar v_F \sqrt{\kappa(n)^2 + k^2} \quad (23)$$

with  $\kappa(n) = 2\pi n/L$ .  $s=+1$  for the energy levels in the conduction band  $\epsilon > 0$  and  $s=-1$  for the energy levels in the valence band  $\epsilon < 0$ .  $N$  is given by the number of unit cells and  $M$  is the mass of a carbon atom. The subtraction of the last term in Eq. (21) is due to the fact that in order to calculate the frequency shift for nanotubes, we insert in the calculated expressions the known optical frequencies of graphene which then results in a double counting when we only use the first term in Eq. (21) as self-energy.<sup>35</sup> The valley degeneracy is here considered by a factor 2 in correspondence to similar expressions in Ref. 35. The upper sign corresponds to the self-energy of longitudinal phonons  $\Pi^L$ , the lower sign to the transversal ones  $\Pi^T$ .

In the case of the frequency shift of the longitudinal and transversal optical  $\Gamma$  mode Ishikawa *et al.* use the zero-temperature Fermi function for  $f[\epsilon^s(n,k)]$ . The frequency shift  $\Delta\omega$  and broadening  $\Gamma$  is given by<sup>35</sup>

$$\Delta\omega = \text{Re}[\Pi(\omega^\Gamma)], \quad \Gamma = -\text{Im}[\Pi(\omega^\Gamma)]. \quad (24)$$

In Ref. 35 it is then shown that this leads to a good agreement of the theoretically calculated frequency shifts and broadenings by using Eqs. (21)–(24) and the experimentally determined ones using Raman spectroscopic methods. In the following, we carry out a similar calculation for the case of the electron system under high bias voltage. For this we use for  $f[\epsilon^s(n,k)]$  in Eq. (22) for the lowest energy band, i.e.,  $n=0$ , the distribution functions  $f_L$  and  $f_R$  calculated in the last section. For the higher bands  $n \neq 0$  we shall use the Fermi function since we did not take into account higher band excitations in Sec. IV being negligible in the considered voltage regime.

$$f[\epsilon^s(n,k)] = \begin{cases} f_L(k) & \text{for } n=0 \text{ and } k \cdot s < 0 \\ f_R(k) & \text{for } n=0 \text{ and } k \cdot s > 0 \\ n_F[\epsilon^s(n,k)] & \text{for } n \neq 0 \end{cases}. \quad (25)$$

Expression (22) for the phonon self-energy corresponds to a current-current Green's-function loop being the lowest-order approximation for the phonon self-energy. When using dressed Green's functions by taking into account the electron-phonon interaction and also the external electric field one has to use nonequilibrium Green's-function techniques in order to get the corresponding loop expression<sup>36</sup> for the retarded phonon self-energy. The relevant Green's functions in the loop are given by lesser  $G^<$  and greater Green's functions  $G^>$ . We now express these Green's functions by the spectral function and use the quasiparticle approximation<sup>36</sup> established for deriving the Boltzmann equation. This leads to Eqs. (21) and (22) with Eq. (25).

It is well known that, by using the free Green's function in loops as was done by Ishikawa *et al.*,<sup>35</sup> this approximation is conserved<sup>37</sup> which means that the charge-current response functions corresponding to the loop fulfill the continuity equation.<sup>37</sup> By using a more general dressed Green's function in the loop one needs also vertex corrections in order to fulfill the continuity equation. It is straightforward to show that the current-density correlation functions corresponding to Eqs. (21) and (22) with Eq. (25) which consist of dressed Green's function in loops with the additional quasiparticle approximation does indeed fulfill the continuity equation. This justifies approximations (21) and (22) with Eq. (25) for the phonon self-energy at zero momentum to calculate the phonon self-energy under high bias voltage.

In the following, we use the abbreviations

$$\tilde{\omega} = \omega \frac{\pi D}{2\pi v_F}, \quad (26)$$

$$\alpha(D) = \frac{27}{\pi} \beta^2 \left[ \frac{2(\hbar v_F)}{\sqrt{3}} \right] \frac{\hbar^2}{2Ma^3} \left( \frac{1}{\hbar \omega^\Gamma} \right)^2 \frac{a}{\pi D}. \quad (27)$$

Here  $a$  is  $\sqrt{3}$  times the equilibrium bond length. With the knowledge of the parameter  $\tau_{\text{ep}}^\Gamma = 538$  fs determined by density functional methods for a nanotube of diameter 2 nm (Ref. 11) we are able to determine  $\beta$  and thus  $\alpha(D)$ . By using that  $\tau_{\text{ep}}^\Gamma$  is more generally proportional to the diameter of the nanotube<sup>10</sup> we obtain from Eq. (27) that

$$\alpha(D) \approx 0.1a/\pi D. \quad (28)$$

With the help of Eqs. (21), (22), and (25) by using the abbreviation  $\Pi^L(\omega) = \Pi_{U=0}^L(\omega) + \Pi_{U>0}^L(\omega)$  we obtain

$$\Pi^T(\omega) = \alpha(D)\omega^\Gamma \left( 2 - \frac{\pi^2}{9}\tilde{\omega}^2 \right), \quad (29)$$

$$\Pi_{U=0}^L(\omega) = \alpha(D)\omega^\Gamma \left( 2 \ln \frac{2\pi\tilde{\omega}}{e} - \frac{\pi^2}{18}\tilde{\omega}^2 - i\pi \right). \quad (30)$$

$\Pi_{U>0}^L$  is a correction factor to the zero-bias self-energy  $\Pi_{U=0}^L$  [Eq. (30)]. By taking into account that  $\Pi^T(n=0, \omega) = 0$  [Eq. (22)] we obtain that this factor is of similar order as the zero-bias self-energy only in the longitudinal sector for  $eU \ll \hbar v_F 2/D$ . Note that we restrict here ourselves also to the regime  $eU \ll \hbar v_F 2/D$  as was done in the last sections by taking into account that excitations to higher bands are negligible. We obtain for the self-energy  $\Pi_{U>0}^L$

$$\Pi_{U>0}^L(\omega, x) = \Pi_1^L(\omega, x) + \Pi_2^L(\omega, x) \quad (31)$$

with

$$\Pi_1^L(\omega, x) = \alpha(D)\omega^\Gamma \left\{ 2C(\tilde{x}) + 2 \ln \left( \frac{2eU}{\hbar \omega} \right) + i\pi \right\}, \quad (32)$$

$$\begin{aligned} \Pi_2^L(\omega, x) \approx & -\alpha(D)\omega^\Gamma \frac{1}{2} \left\{ (1-\tilde{x}) \ln \left( \frac{\left| \tilde{x} + \frac{\hbar \omega L}{eU\pi l_{\text{sc}}} \right|}{\tilde{x}} \right) \right. \\ & \left. + \tilde{x} \ln \left( \frac{\left| 1 - \tilde{x} - \frac{\hbar \omega L}{eU\pi l_{\text{sc}}} \right|}{1-\tilde{x}} \right) \right\} \\ & + \left\{ \frac{\hbar \omega L}{eU\pi l_{\text{sc}}} \rightarrow -\frac{\hbar \omega}{eU\bar{n}} \right\}, \end{aligned} \quad (33)$$

where

$$C(x) \equiv x \ln(1-x) + (1-x)\ln(x) \quad (34)$$

and  $\tilde{x} \equiv x/L$ . The last line in Eq. (33) means that we have to add the foregoing expressions with the substitution  $(\omega/\pi)L/l_{\text{sc}} \rightarrow -\omega\bar{n}$ . Here  $\Pi_1^L$  is the self-energy part calculated by the help of  $f^{t=0}$  [Eq. (A6)] in Eq. (22).  $\Pi_2^L$  is the result for  $f^{t \neq 0}$  [Eq. (A11)]. In Eq. (33) we carry out for the logarithmic term in the electron distribution function (A9) the approximation that we set this term constant over the range

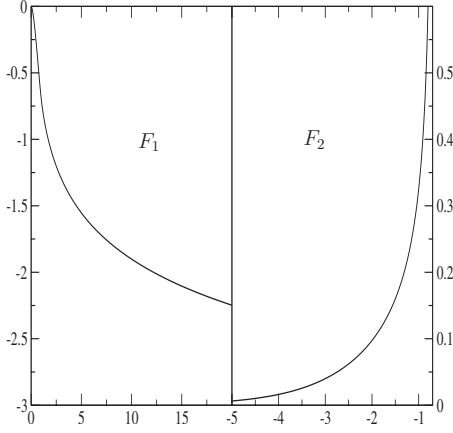


FIG. 8. The left panel shows the function  $F_1(x)$  [Eq. (38)]. On the right hand side we show the Raman lineshape function  $F_2(x)$  defined in Eq. (39).

$\pi|\epsilon - eEx_1|l_{sc}/\hbar\omega L < 1$  with its value at  $|\epsilon - eEx_1| = 0$  and zero elsewhere. This approximation leads to the logarithmic singularities in Eq. (33). They are softened when using the exact functions  $f_L^{i \neq 0}$  [Eq. (A11)] without approximation but this treatment has the disadvantage that we would not obtain analytical results. We should additionally mention that we neglect those imaginary terms in Eqs. (32) and (33) which exist only in small regions in position space of length  $\Delta x = L\hbar\omega/eU$ . These correspond to regions where the  $\ln$  terms in Eqs. (32) and (33) gets singular.

By taking into account the results in Eqs. (30)–(33) we obtain the surprising result that the imaginary part of the longitudinal phonon self-energy and thus the level broadening vanishes

$$\text{Im}[\Pi^L(\omega, x)] = 0 \quad (35)$$

in the high voltage-bias regime  $eU \gg \hbar\omega$  in contrast to the case of no bias [Eq. (30)]. The reason for this vanishing is seen in Eq. (22). We only obtain an imaginary part for the phonon self-energy when there is a substantial changing of the electron distribution function in the energy range  $|2\epsilon| < \hbar\omega$ . In the high bias regime the electron distribution function (25) becomes constant in this range which is not the case for the Fermi function in the zero-bias system.

### A. Position-averaged self-energy

Finally we calculate the position averaged self-energy  $\bar{\Pi}_i^L = \int dx \Pi_i^L(\omega, x)/L$ . We obtain

$$\bar{\Pi}_1^L(\omega) = \alpha(D)\omega^\Gamma \left[ -3 + 2 \ln\left(\frac{2eU}{\hbar\omega}\right) + i\pi \right], \quad (36)$$

$$\bar{\Pi}_2^L(\omega) \approx \alpha(D)\omega^\Gamma \left[ F_1\left(\frac{\hbar\omega}{\pi eU l_{sc}}\right) + F_1\left(\frac{\hbar\omega}{eU \bar{n}}\right) \right] \quad (37)$$

with

$$F_1(x) = \frac{1}{4}(x+1)^2[\ln(|x|) - \ln(|1+x|)] - \frac{1}{4}\ln(|x|) + (x \rightarrow -x). \quad (38)$$

We show in Fig. 8 the function  $F_1(x)$ . In the regime of very high voltages  $eUl_{sc}/L \gg \hbar\omega/\pi$  we obtain that  $\bar{\Pi}_2^L(\omega)$  is negligible in comparison to  $\bar{\Pi}_1^L(\omega)$ . For nanotubes of diameter 2 nm we have  $\bar{\omega}_0 \approx 0.35$ . Thus we obtain that  $\text{Re}[\Pi_{U=0}^L(\omega^\Gamma)] \approx -0.46\alpha(D)\omega^\Gamma$  leading to the result that  $\text{Re}[\Pi^L(\omega^\Gamma)] \approx \alpha(D)\omega^\Gamma[-3.48 + 2 \ln(2eU/\hbar\omega^\Gamma)]$ . This means that we obtain in the high-voltage regime for  $eU/\hbar\omega^\Gamma \gtrsim 1.8$  a positive frequency shift for the longitudinal optical phonon frequency at the  $\Gamma$  point. On the other hand, by taking into account that  $\lim_{x \rightarrow \infty} F_1(x) = -1/2 \ln(x)$  we obtain that for fixed  $eU/\hbar\omega^\Gamma$  and in the large length limit  $L/l_{sc} \rightarrow \infty$  where  $\bar{n} \leq 1$ , that the frequency shift is negative.

### B. Lineshape of Raman signal

From the considerations above it is not clear how the actual lineshape of the Stokes or anti-Stokes signal looks like in an actual Raman-scattering experiment. From above we obtain first that the Raman signal corresponding to the response on transversal phonon mode excitations denoted by  $G^+$  is not changed from the zero-bias result. This is not true for the  $G^-$  Raman mode corresponding to the response on longitudinal optical phonons. In order to get a better insight into the actual Raman lineshape we assume that the incident laser light illuminates the nanotube continuously over the whole width. In typical Raman experiments the scattering of the electron system with the incident light is dominated by the resonant scattering of a valence band and conduction band of fixed index  $n > 0$  [Eq. (23)].<sup>38</sup> A further enhancement of the signal is reached when electrons from the band edges are scattered. This is due to the Van Hove singularities of the density of states at this region leading not until then to the opportunity of measuring phonon and electronic properties of single nanotubes. Further let us assume in a first approximation that the phonon distribution function  $n^\Gamma(x)$  [Eq. (8)] is homogeneous over the nanotube width which was also assumed in our analytical calculations in Sec. IV. This leads us to the conclusion by taking into account that only the electron distribution function of the lowest electronic energy band  $n=0$  is changed due to the large bias voltage that we can determine at least approximately the lineshape of an actual Raman signal by the position average over the individual Raman signals.

In the following, we use the abbreviation

$$F_2(x) = \int_0^1 dy \delta[C(y) - x] \quad (39)$$

in order to calculate the lineshape of the Raman signal. We restrict ourselves in the following to the most important high bias regimes  $\pi eUl_{sc}/L \gg \hbar\omega^\Gamma$  and to the large length regime where  $\pi eUl_{sc}/L \ll \hbar\omega^\Gamma$ , but  $eU \gg \hbar\omega^\Gamma \bar{n}$  where we obtain simple expression for the Raman signal. By taking into account that  $\text{Im}[\Pi^L] = 0$  we obtain for the lineshape of Stokes and anti-Stokes signal  $I_{ep}$  by using Eqs. (32), (33), and (39)

$$I_{\text{ep}}(\omega) \propto \begin{cases} \frac{1}{2}F_2 \left\{ \frac{\omega - \omega^\Gamma - \text{Re}[\Pi_{U=0}^L(\omega^\Gamma)]}{2\alpha(D)\omega^\Gamma} - \ln\left(\frac{2eU}{\hbar\omega^\Gamma}\right) \right\} & \text{for } \frac{eU}{\hbar\omega^\Gamma} \gg \frac{L}{\pi l_{\text{sc}}} \\ \frac{2}{5}F_2 \left\{ \frac{\omega - \omega^\Gamma - \text{Re}[\Pi_{U=0}^L(\omega^\Gamma)]}{(5/2)\alpha(D)\omega^\Gamma} - \frac{4}{5}\ln\left(\frac{2eU}{\hbar\omega^\Gamma}\right) + \frac{1}{5}\ln\left(\frac{\hbar\omega^\Gamma L}{\pi eU l_{\text{sc}}}\right) \right\} & \text{for } \bar{n} \ll \frac{eU}{\hbar\omega^\Gamma} \ll \frac{L}{\pi l_{\text{sc}}} \end{cases} \quad (40)$$

We show on the right-hand side in Fig. 8 the function  $F_2$ . Due to the maximum of  $C(x)$  at  $x=1/2$  with  $C(1/2)=-\ln(2)$  we obtain that  $F_2(x)$  is singular at  $x=-\ln 2$ . This singularity leads to a sharp edge of the Raman spectrum at the corresponding frequency according to Eq. (40).

By taking into account also the broadening of the phonon modes due to the phonon-phonon scattering we obtain that the signal of the actual Raman mode is a convolution of  $I_{\text{ep}}(\omega)$  [Eq. (40)] with a Lorentzian which has a negative frequency shift and broadening corresponding to the phonon-phonon interaction contribution to the phonon self-energy.

### C. Discussion

Next we compare our findings with recent experiments. In Refs. 9 and 21 the optical phonon lifetimes and frequency shifts are measured for *suspended* metallic carbon nanotubes at high bias voltage using Raman spectroscopy. These investigations did not find a response of the  $G_-$  and  $G_+$  modes corresponding to the longitudinal and transversal optical  $\Gamma$  modes for all measured nanotubes where only the former mode couples to the electron system at high bias. In fact, it is not well understood which mode response to the bias for a certain nanotube. The nanotube phonon temperature was then measured by two different methods either by the Stokes/anti-Stokes intensity ratio being a function of the phonon Boltzmann factor of the corresponding mode or by mode softening where one compares the softened mode with the known temperature softening which is caused by phonon-phonon scattering. Astonishing, that both methods find phonon temperatures which are in good accordance. They did not provide any hint for a different behavior which we found theoretically above.

Such a different behavior was in fact seen by Oron-Carl *et al.*<sup>6</sup> for metallic nanotubes on a  $\text{SiO}_2$  substrate. They found a mode hardening and a reduction in the linewidth at high bias voltage in comparison to the zero-bias voltage values. A real quantitative comparison of our results with the experimental finding is difficult here since the overall broadening and hardening is the additive effect of phonon-phonon scattering leading to softening and broadening of the mode and the hardening effect and a linewidth reduction due to the electron-phonon coupling. That this nonthermal effect was not seen in free-standing nanotubes could be explained by the fact that the heating of many of the crystal modes are much easier for phonons in a suspended crystal in comparison to phonons on a substrate since these phonons could travel especially in long nanotubes substantially until they

diffuse out of the system. This is the reason for the experimental finding that large nanotubes show a bias response for the  $G_+$  mode and the  $G_-$  mode in general.<sup>21</sup> During this traveling the electron-scattered optical phonons are then thermalized by scattering with acoustic phonons. A true understanding of the different behavior of the frequency shift and broadening between suspended nanotubes and nanotubes on a substrate requires a distinct theory for suspended nanotubes being out of the scope of this work.

### VI. SUMMARY

In this paper we have used the coupled Boltzmann equations for electrons and optical phonons to calculate the current-voltage characteristic of carbon nanotubes lying on a substrate under high bias voltage. First we have studied the coupled electron-phonon Boltzmann system. By taking into account the electron-phonon relaxation time of Ref. 10 which agrees well with experiments, we have determined by numerical fitting the relaxation times of the optical phonons in the single-mode relaxation-time approximation. These are much longer for short nanotubes below 1  $\mu\text{m}$  than for large ones. The result was obtained by fitting our numerically determined current-voltage curves with the experiments. For short nanotubes, this time did not agree with experimental findings. In Sec. III we went beyond the single time relaxation approximation by taking into account also lower-lying secondary phonons in the Boltzmann equation which leads us to the conclusion that the phonon relaxation shows a bottleneck in the sector of acoustic phonons for short nanotubes but not for long nanotubes. We have explained this by the fact that due to the phonon velocity of the lower-lying acoustic phonons, these phonons are redistributed in such a way that at least locally a bottleneck is created for short nanotubes. This leads to a plug in the relaxation path of the optical phonons.

In Sec. IV, we have considered an analytical solution of the Boltzmann system where we first linearize the electronic equations and use further the assumption of a constant phonon distribution function to solve them in the electronic sector. We have compared our results for the current-voltage characteristic and the phonon distribution function with the numerical findings of Sec. II, Sec. III, and the experimental results. We find an especially good agreement in the high-voltage, small-length regime. Our analytical theory provides us with the electron and phonon distribution functions as a function of position and momentum. This opens the possibility to calculate the optical phonon broadening and frequency

shift due to the coupling of the phonon system to the bias-driven electronic system. For zero bias this coupling is the dominant contribution for both quantities.

We have then calculated in Sec. V in a charge-current conserved way the broadening and frequency shift of the zone-center optical phonons. We find that the phonon-level broadening, determined at zero-bias voltage mainly by the electron-phonon coupling, vanishes at large voltage. The vanishing was explained by a smoothing of the electron distribution function over the Fermi level at nonzero bias voltage. For very large voltages and small nanotubes, we found a positive frequency shift. Note that this behavior of a vanishing broadening and positive frequency shift is in contrast to the self-energy contribution of the phonon-phonon interaction to the lower-lying hot acoustic phonons. This contribution to the self-energy led to a negative frequency shift and an additional broadening at higher bias due to a temperature increase in the lower-lying acoustic phonons.

It was in fact just recently found experimentally by Raman scattering, that the level broadening decreases and the frequency shift increases for the zone-center optical phonons<sup>6</sup> for increasing bias voltage. In contrast to the very high-voltage regime, we found a negative frequency shift at moderate bias voltage and large nanotubes.

#### ACKNOWLEDGMENTS

The authors acknowledge the useful discussions with V. Bezerra, M. Lazzeri, C. Auer, F. Schürer, and C. Ertler. We further acknowledge the support provided by Deutsche Forschungsgemeinschaft under Grant No. KL 256/42-3.

#### APPENDIX: ANALYTIC CALCULATION OF THE CURRENT-VOLTAGE CHARACTERISTIC

In the following, we carry out the calculation of the current-voltage characteristic and the electron-phonon distribution functions for  $eU \gg \hbar\omega$  explicitly by using Eqs. (1)–(7). To solve the system of equations we use the approximations (18) and (19).

##### 1. Current-voltage characteristic

In the following calculation we go in Fourier space  $f_{L/R}(k_{L/R}, x) = 1/(2\pi)^2 \int dk dt \hat{f}_{L/R}(t, k) \exp[i(-kx \mp t v_F \hbar k_{L/R})]$  and use further the function  $\hat{f}_{L/R}$  defined by  $f_{L/R}(k_{L/R}, x) = 1/(2\pi) \int dt \hat{f}_{L/R}(t, x) \exp[\mp i(t v_F \hbar k_{L/R})]$ . With the help of

$$st = \sqrt{1 - \left[ \frac{2\bar{n} \cos(\omega t) + \exp(-i\omega t)}{2\bar{n} + 1} \right]^2} \quad (A1)$$

we obtain from Eq. (1)

$$\hat{f}_L = \frac{\hat{n}_F(t)}{De} \left\{ e^{-ieE(x-L)t/\hbar} \left[ st \cosh\left(\frac{|x|}{l'_{sc}} st\right) + \sinh\left(\frac{|x|}{l'_{sc}} st\right) \right] + e^{-ieExt/\hbar} (1-st^2)^{1/2} \sinh\left(\frac{|x-L|}{l'_{sc}} st\right) \right\} \quad (A2)$$

with

$$De = st \cosh\left(\frac{L}{l'_{sc}} st\right) + \sinh\left(\frac{L}{l'_{sc}} st\right), \quad (A3)$$

where  $\hat{n}_F(t)$  is the Fourier transform of the Fermi function, i.e.,  $\hat{n}_F(t) = \int d\epsilon n_F(\epsilon) \exp[-it\epsilon] = +i/(t+i\delta)$ . The function  $f_R$  is given by Eqs. (A2) and (A3) with the substitution

$$f_R = f_L[x \rightarrow x-L, x-L \rightarrow x]. \quad (A4)$$

We note that one has to take into account during this substitution the absolute value signs in the cosine hyperbolic and sinus hyperbolic arguments in Eq. (A2).

In the following, we evaluate Eq. (A2) by the help of a residuum integration. With

$$f_L = f_L^{t=0} + f_L^{t \neq 0} \quad (A5)$$

we obtain for the electron distribution function  $f_L^{t=0}$  due to the residuum at  $t=0$

$$f_L^{t=0} = \{1 - n_F[\epsilon - eE(x-L)]\} + \{n_F(\epsilon - eEx) - n_F[\epsilon - eE(x-L)]\} \frac{|x-L|}{l'_{sc}} \frac{1}{1 + \frac{L}{l'_{sc}}}. \quad (A6)$$

$f_R^{t \neq 0}$  is given by Eq. (A6) with the substitution (A4). The  $t \neq 0$  singularities are given by the zeros of  $De$ . For  $L/l'_{sc} \gg 1$  we obtain for these zeroes

$$st \approx i \frac{\pi n}{\left(1 + \frac{L}{l'_{sc}}\right)} \quad \text{for } |st| \lesssim 1, \quad (A7)$$

$$st \approx i \left( \pi n - \frac{\pi}{2} \right) \frac{l'_{sc}}{L} \quad \text{for } |st| \gtrsim 1. \quad (A8)$$

With the help of

$$A_1(x_1, x_2) = \frac{1}{2\pi i} \left\{ [1 - n_F(\epsilon - eEx_1)] - n_F(\epsilon - eEx_1) \exp\left(-\frac{1}{\bar{n}} \frac{1}{\omega} |\epsilon - eEx_1|\right) \right\} \times \sum_{\pm} \pm \ln \left[ 1 + \exp \left[ -\frac{\pi}{\left(1 + \frac{L}{l'_{sc}}\right)} \left( \frac{|\epsilon - eEx_1|}{\omega} \pm i \frac{|x_2|}{l'_{sc}} \right) \right] \right], \quad (A9)$$

$$A_2(x_1, x_2) = \frac{1}{2 \left(1 + \frac{L}{l_{sc}^r}\right)} \left\{ [1 - n_F(\epsilon - eEx_1)] - n_F(\epsilon - eEx_1) \exp\left(-\frac{1}{\bar{n}} \frac{1}{\omega} |\epsilon - eEx_1|\right) \right\} \\ \times \sum_{\pm} \left\{ 1 + \exp\left[\frac{\pi}{\left(1 + \frac{L}{l_{sc}^r}\right)} \left(\frac{|\epsilon - eEx_1|}{\omega} \pm i \frac{|x_2|}{l_{sc}^r}\right)\right] \right\}^{-1} \quad (\text{A10})$$

we obtain for  $f^{t \neq 0}$  due to the singularities in the regime  $|st| \geq 1$  Eq. (A7)

$$f_L^{t \neq 0} = A_1(x, x-L) + A_1(x-L, x) + A_2(x-L, x). \quad (\text{A11})$$

$f_R^{t \neq 0}$  is given by  $f_L^{t \neq 0}$  with the substitution (A4).

Finally, we have to discuss the contribution of singularities  $|st| \geq 1$  [Eq. (A8)] to  $f^{t \neq 0}$ . Due to the Fourier exponent, these terms are exponentially suppressed beyond a small energy strip of range  $|\Delta\epsilon|/\omega \geq 1$  in comparison to terms calculated with residual  $|st| \leq 1$ . From the discussion above and the following discussions we obtain that these terms are not relevant in the range  $eU/\hbar\omega \gg 1$ ,  $L \gg l_{sc}^r$  for the determination of the phonon distribution function. We also note without an explicit calculation here but which can be shown with similar methods as for the current calculation of the  $|st| \leq 1$  singularities below that the current from the  $|st| \geq 1$  singularities is negligible in comparison to the current calculated from the singularities  $|st| \leq 1$ . This current contribution will be calculated explicitly in the following.

The current  $I$  can be calculated by the help of  $I = (4e/h) \int d\epsilon (f_R - f_L)$ . This is best done by carrying out the integration at the boundaries  $x=0$  or  $x=L$  of the nanotube. From Eqs. (A6) and (A11) and the corresponding expressions for  $f_R$ , we obtain the following current-voltage characteristic:

$$I = 4 \frac{e}{h} \left[ \hbar\omega B_1 \left( \frac{1 + \frac{L}{l_{sc}^r}}{\pi\bar{n}} \right) + e \frac{U}{\left(1 + \frac{L}{l_{sc}^r}\right)} \right] \quad (\text{A12})$$

with

$$B_1(x) = \frac{1}{2\pi} \left[ H\left(\frac{x}{2} - 1\right) - H\left(\frac{x}{2}\right) + \ln(4) + 2H(x) \right], \quad (\text{A13})$$

where  $H(x) = \gamma + \Psi(x+1)$  and  $\gamma$  is the Euler-Mascheroni constant,  $\Psi(x)$  is the digamma function. We show in Fig. 6 the function  $B_1(x)$ .

## 2. Phonon distribution function

Next we calculate the phonon distribution function  $\bar{n}(x)$  [Eq. (15)]. We carry out this calculation only in the leading order in  $l_{sc}^r/L$ . In order to simplify our notation we define  $\tilde{x} \equiv x/L$ . Next we calculate from Eqs. (A6) and (A11) and the

corresponding equation for  $f_R$  [Eq. (A4)] the phonon distribution function in the regime  $\pi eU \gg \hbar\omega L/l_{sc}$

### a. Phonon distribution function for $\pi eU \gg \hbar\omega L/l_{sc}$

In the following, we only have to determine the  $k > 0$  phonons since we find from symmetry arguments that

$$n(k, x) = n(-k, -x). \quad (\text{A14})$$

To simplify our notation we define the following regimes for  $k > 0$ :

$$\mathcal{R}_1: \tilde{x} < \frac{1}{2}, eU(1 - \tilde{x}) > \frac{v_F \hbar k}{2} > eU\tilde{x},$$

$$\mathcal{R}_2: \tilde{x} > \frac{1}{2}, eU\tilde{x} > \frac{v_F \hbar k}{2} > eU(1 - \tilde{x}),$$

$$\mathcal{R}_3: \tilde{x} < \frac{1}{2}, eU\tilde{x} > \frac{v_F \hbar k}{2} \text{ or } \tilde{x} > \frac{1}{2}, eU(1 - \tilde{x}) > \frac{v_F \hbar k}{2}. \quad (\text{A15})$$

We obtain for the phonon-Boltzmann Eq. (4) by using Eqs. (A4), (A6), and (A11)

$$\frac{\partial}{\partial x} n(k, x) = K_1 n(k, x) + K_2 \quad (\text{A16})$$

with

$$\mathcal{R}_1: K_1 = -\frac{1}{v_{ph}} \left( \frac{s^p l_{sc}}{\tau_{ep} L} + \frac{1}{\tau_{op}} \right), K_2 = \frac{s^p \tilde{x}}{v_{ph} \tau_{ep}},$$

$$\mathcal{R}_2: K_1 = -\frac{1}{v_{ph}} \left( -\frac{s^p l_{sc}}{\tau_{ep} L} + \frac{1}{\tau_{op}} \right), K_2 = \frac{s^p (1 - \tilde{x})}{v_{ph} \tau_{ep}},$$

$$\mathcal{R}_3: K_1 = -\frac{1}{v_{ph} \tau_{op}}, K_2 = 2 \frac{s^p \tilde{x} (1 - \tilde{x})}{v_{ph} \tau_{ep}}. \quad (\text{A17})$$

By taking into account the boundary conditions  $n(k, 0) = 0$  and further  $v_{ph} \tau_{op} \ll L$  we obtain for  $n(k, x)$  in  $\mathcal{R}_1$  and  $\mathcal{R}_3$

$$\mathcal{R}_1: n_{\mathcal{R}_1}(k, x) = -\frac{s^p L}{v_{ph} \tau_{ep} K_1 L} \tilde{x}, \quad (\text{A18})$$

$$\mathcal{R}_3:n_{\mathcal{R}_3}(k,x) = -\frac{s^p L}{v_{\text{ph}}\tau_{\text{ep}} K_1 L} 2\tilde{x}(1-\tilde{x}). \quad (\text{A19})$$

We point out here that according to Eq. (A17) the expressions for  $K_1$  in Eqs. (A18) and (A19) are different in the different regimes [Eq. (A15)]. We obtain in these regions the same solutions  $n(k,x)$  of Eq. (2) as we would set immediately  $v_{\text{ph}}=0$  from the beginning. This is not true for  $n(k,x)$  in  $\mathcal{R}_2$ . We obtain especially in the regions where  $l_{\text{sc}}/L \sim \tau_{\text{ep}}/\tau_{\text{op}}$  that the neglect of the  $v_{\text{ph}}$  term in Eq. (2) is not allowed. Such parameter values lead to the result that the phonon distribution function at the boundary of the nanotube increases which is in fact seen in Fig. 5. In the regime  $\mathcal{R}_2$  we obtain from Eqs. (A16) and (A17)

$$\begin{aligned} \mathcal{R}_2:n_{\mathcal{R}_2}(k,x) &= n_0[k,x_0(k)]e^{K_1[x-x_0(k)]} + \frac{s^p L}{v_{\text{ph}}\tau_{\text{ep}} K_1 L} \\ &\times \left\{ \frac{1}{K_1 L} (1 + K_1 x) - e^{K_1[x-x_0(k)]} \right. \\ &\left. \times \frac{1}{K_1 L} [1 + K_1 x_0(k)] \right\}, \quad (\text{A20}) \end{aligned}$$

where  $x_0(k) = L(1/2 + |1/2 - v_F \hbar k / 2eU|)$ ,  $n_0[k, x_0(k)] = n_{\mathcal{R}_3}[k, x_0(k)]$  for  $v_F \hbar k / 2 < eU/2$  and  $n_0[k, x_0(k)] = 0$  for  $v_F \hbar k / 2 > eU/2$ .

We now use the abbreviation

$$\tilde{K}_1 = K_1 L. \quad (\text{A21})$$

Next, we calculate the phonon density  $\bar{n}(x)$  [Eq. (15)]. According to the discussion above, we obtain

$$\begin{aligned} \bar{n}(x) &\approx [\bar{n}_{\mathcal{R}_1}(L-x) + \bar{n}_{\mathcal{R}_2}(x)]\theta(\tilde{x}-1/2) + [\bar{n}_{\mathcal{R}_1}(x) \\ &+ \bar{n}_{\mathcal{R}_2}(L-x)]\theta[1-(\tilde{x}-1/2)] + 2\bar{n}_{\mathcal{R}_3}(x), \quad (\text{A22}) \end{aligned}$$

where  $\bar{n}_{\mathcal{R}_i}$  are the energy averaged phonon distribution functions (A18)–(A20) according to Eq. (15) where the integration region are restricted to  $\mathcal{R}_i$  [Eq. (A15)]. These are given by

$$\bar{n}_{\mathcal{R}_1}(x) = -\frac{1}{2} \frac{s^p L}{v_{\text{ph}}\tau_{\text{ep}} \tilde{K}_1} \tilde{x}(1-2\tilde{x}), \quad (\text{A23})$$

$$\bar{n}_{\mathcal{R}_3}(x) = -\frac{s^p L}{v_{\text{ph}}\tau_{\text{ep}} \tilde{K}_1} \left( \frac{1}{2} - \left| \tilde{x} - \frac{1}{2} \right| \right) \tilde{x}(1-\tilde{x}), \quad (\text{A24})$$

and

$$\begin{aligned} \bar{n}_{\mathcal{R}_2}(x) &\approx \frac{s^p L}{v_{\text{ph}}\tau_{\text{ep}} \tilde{K}_1} \left\{ \left( \tilde{x} - \frac{1}{2} \right) (\tilde{x}-1) + \frac{1}{\tilde{K}_1} \left[ \left( 2\tilde{x} - \frac{3}{2} \right) \right. \right. \\ &\left. \left. + \frac{1}{2} e^{\tilde{K}_1(\tilde{x}-1/2)} \right] + \frac{2}{\tilde{K}_1^2} (1 - e^{\tilde{K}_1(\tilde{x}-1/2)}) \right\}, \quad (\text{A25}) \end{aligned}$$

where we took into account that  $L/v_{\text{ph}}\tau_{\text{op}} \gg 1$ . Finally, we calculate the position-averaged phonon distribution function  $\bar{n} = \int dx \bar{n}(x)/L$ . We obtain

$$\bar{n} \approx 2(\bar{n}_{\mathcal{R}_1} + \bar{n}_{\mathcal{R}_2} + \bar{n}_{\mathcal{R}_3}) \quad (\text{A26})$$

with

$$\bar{n}_{\mathcal{R}_1} \approx -\frac{s^p L}{v_{\text{ph}}\tau_{\text{ep}} \tilde{K}_1} \frac{1}{48}, \quad (\text{A27})$$

$$\bar{n}_{\mathcal{R}_3} \approx -\frac{s^p L}{v_{\text{ph}}\tau_{\text{ep}} \tilde{K}_1} \frac{13}{192}, \quad (\text{A28})$$

and

$$\bar{n}_{\mathcal{R}_2} \approx \frac{s^p L}{v_{\text{ph}}\tau_{\text{ep}} \tilde{K}_1} \left[ -\frac{1}{48} + \frac{1}{\tilde{K}_1^2} + \left( \frac{1}{2\tilde{K}_1^2} - \frac{2}{\tilde{K}_1^3} \right) (e^{\tilde{K}_1/2} - 1) \right]. \quad (\text{A29})$$

By taking into account the definition of  $\tilde{K}_1$  Eqs. (A17) and (A21) we obtain that Eq. (A26) is the relation which determines the energy-position-averaged phonon distribution function  $\bar{n}$  [Eq. (18)].

Let us first assume that  $\tilde{K}_1 \gg 1$  in region  $\mathcal{R}_2$ . From expression (A29) we find that there is no solution in this parameter region for Eq. (A26) since  $L/v_{\text{ph}}\tau_{\text{ep}} \gg 1$  and  $v_F\tau_{\text{ep}} = 130$  nm.

Next we assume that  $\tilde{K}_1 \ll -1$  in the region  $\mathcal{R}_2$ . From Eq. (A17) we find then that  $\tilde{K}_1 \approx -L/v_{\text{ph}}\tau_{\text{op}}$  in the regions  $\mathcal{R}_i$ . By using Eq. (A26) we obtain

$$\bar{n} \approx \frac{13}{96} \frac{s^p \tau_{\text{op}}}{\tau_{\text{ep}}} \text{ for } L \gg \frac{v_{\text{ph}}\tau_{\text{ep}}}{\frac{26s^p\tau_{\text{op}}}{96\tau_{\text{ep}}} + 1} \left( \frac{s^p\tau_{\text{op}}}{\tau_{\text{ep}}} - 1 \right). \quad (\text{A30})$$

For  $\tau_{\text{op}} = 9.1$  ps we obtain  $\bar{n} = 5.3$ . This leads to  $l_{\text{sc}} = 11.1$  nm. This value is in excellent agreement with the experimentally determined value  $l_{\text{sc}} \approx 10-11$  nm.<sup>3,4</sup> From Eqs. (A22)–(A25) we obtain that the phonon distribution function  $\bar{n}(x)$  is zero at the boundary of the nanotube. By using the scattering parameters in Eq. (14) we further obtain the validity of Eq. (A30) for  $L \gg 426$  nm.

For smaller nanotube lengths one has  $\tilde{K}_1 \sim 0$ . By explicit calculation we obtain for  $L/v_{\text{ph}}\tau_{\text{op}} \gg 1$  and  $\tilde{K}_1 \sim 0$  that  $\bar{n}_{\mathcal{R}_1}, \bar{n}_{\mathcal{R}_3} \ll \bar{n}_{\mathcal{R}_2}$ . By taking only  $\bar{n}_{\mathcal{R}_2}$  into account in Eqs. (A22) and (A26) we obtain for the energy-averaged phonon distribution function by Taylor expanding Eq. (A25) with respect to  $\tilde{K}_1$

$$\bar{n}(x) \approx \frac{s^p L}{v_{\text{ph}}\tau_{\text{ep}}} \left( \frac{1}{4} |\tilde{x} - 1/2|^2 - \frac{1}{3} |\tilde{x} - 1/2|^3 \right) \quad (\text{A31})$$

and for Eq. (A26) with Eq. (A29)

$$\bar{n} \approx \frac{s^p L}{v_{\text{ph}}\tau_{\text{ep}}} \frac{1}{96}. \quad (\text{A32})$$

From Eq. (A31) we get an increasing behavior of the phonon distribution function at the boundary of the nanotube in agreement with Fig. 5.

Finally, we calculate the phonon distribution function  $\bar{n}$  by solving Eq. (A26) for  $\bar{n}$  with Eqs. (A27)–(A29) numeri-

cally as a function of the nanotube length  $L$ . The result is shown in Fig. 7. We obtain that the decrease in  $\bar{n}$  in the direction of small  $L$  values given by Eq. (A32) is not quite large so that we can assume approximately the validity of Eq. (A30) in the whole regime  $L \gtrsim 50$  nm. Next, we calculate the phonon distribution function for  $\pi eU \ll \hbar \omega L / l_{sc}$ .

### b. Phonon distribution function for $\pi eU \ll \hbar \omega L / l_{sc}$

By taking into account Eqs. (A4), (A6), and (A11) we obtain that  $n(k, x) \neq n_B^{ac}$  only in the regime  $|\pi(v_F|k|/2\omega)l_{sc}/L| \leq 1$  where we use that  $\bar{n} \leq 1$  as will be shown below. In this regime we obtain for  $k > 0$  [Eq. (A16)] with

$$K_1 = -\frac{1}{v_{ph}} \left\{ \frac{s^p l_{sc}}{\tau_{ep} L} \left[ \frac{\cos(\pi \tilde{x})}{1 - \cos^2(\pi \tilde{x})} \right] + \frac{1}{\tau_{op}} \right\},$$

$$K_2 = \frac{s^p}{4v_{ph}\tau_{ep}}, \quad (\text{A33})$$

where again Eq. (A14) holds. We now assume that  $l_{sc}/L \ll \tau_{ep}/\tau_{op}$  which is good fulfilled in the large length regime where we have Eq. (14)  $\tau_{ep}/\tau_{op} \approx 0.22$ . Then we obtain for  $|\pi(v_F|k|/2\omega)l_{sc}/L| \leq 1$

$$n(k, x) \approx \frac{s^p \tau_{op}}{4 \tau_{ep}}. \quad (\text{A34})$$

We point out that Eq. (A34) is not valid in the small regime where  $0 \leq |\epsilon| \leq eU, \bar{n}\omega$ . We obtain a position-dependent numerical prefactor to Eq. (A34) in this regime. From Eq. (A34) we are able to calculate  $\bar{n}(x)$  and  $\bar{n}$  given by

$$\bar{n}(x) = \bar{n} \approx \frac{s^p \tau_{op}}{4 \tau_{ep}}. \quad (\text{A35})$$

- 
- <sup>1</sup>Z. Yao, C. L. Kane, and C. Dekker, *Phys. Rev. Lett.* **84**, 2941 (2000).
- <sup>2</sup>V. Perebeinos, J. Tersoff, and P. Avouris, *Phys. Rev. Lett.* **94**, 086802 (2005).
- <sup>3</sup>J. Y. Park, S. Rosenblatt, Y. Yaish, V. Sazonova, H. Üstünel, S. Braig, T. A. Arias, P. W. Brouwer, and P. L. McEuen, *Nano Lett.* **4**, 517 (2004).
- <sup>4</sup>A. Javey, J. Guo, M. Paulsson, Q. Wang, D. Mann, M. Lundstrom, and H. Dai, *Phys. Rev. Lett.* **92**, 106804 (2004).
- <sup>5</sup>E. Pop, D. A. Mann, K. E. Goodson, and H. Dai, *J. Appl. Phys.* **101**, 093710 (2007).
- <sup>6</sup>M. Oron-Carl and R. Krupke, *Phys. Rev. Lett.* **100**, 127401 (2008).
- <sup>7</sup>M. Steiner, M. Freitag, V. Perebeinos, J. C. Tsang, J. P. Small, M. Kinsoshita, D. Yang, J. Liu, and P. Avouris, *Nat. Nanotechnol.* **4**, 320 (2009).
- <sup>8</sup>P. Sundqvist, F. J. Garcia-Vidal, F. Flores, M. Moreno-Moreno, C. Gómez-Navarro, J. S. Bunch, and J. Gómez-Herrero, *Nano Lett.* **7**, 2568 (2007).
- <sup>9</sup>A. W. Bushmaker, V. V. Deshpande, M. W. Bockrath, and S. B. Cronin, *Nano Lett.* **7**, 3618 (2007).
- <sup>10</sup>M. Lazzeri, S. Piscanec, F. Mauri, A. C. Ferrari, and J. Robertson, *Phys. Rev. Lett.* **95**, 236802 (2005).
- <sup>11</sup>M. Lazzeri and F. Mauri, *Phys. Rev. B* **73**, 165419 (2006).
- <sup>12</sup>C. Auer, F. Schürer, and C. Ertler, *Phys. Rev. B* **74**, 165409 (2006); *J. Comput. Electron.* **6**, 325 (2007).
- <sup>13</sup>P. A. Sundqvist, F. J. Garcia-Vidal, and F. Flores, *Phys. Rev. B* **78**, 205427 (2008).
- <sup>14</sup>M. A. Kuroda, A. Cangellaris, and J.-P. Leburton, *Phys. Rev. Lett.* **95**, 266803 (2005).
- <sup>15</sup>M. A. Kuroda and J.-P. Leburton, *Phys. Rev. B* **80**, 165417 (2009).
- <sup>16</sup>See, e.g., G. P. Srivastava, *The Physics of Phonons* (Hilger, Bristol, 1990).
- <sup>17</sup>S. Piscanec, M. Lazzeri, F. Mauri, A. C. Ferrari, and J. Robertson, *Phys. Rev. Lett.* **93**, 185503 (2004).
- <sup>18</sup>D. Song, F. Wang, G. Dukovic, M. Zheng, E. D. Semke, L. E. Brus, and T. F. Heinz, *Phys. Rev. Lett.* **100**, 225503 (2008).
- <sup>19</sup>K. Kang, T. Ozel, D. G. Cahill, and M. Shim, *Nano Lett.* **8**, 4642 (2008).
- <sup>20</sup>R. Rao, J. Menendez, C. D. Poweleit, and A. M. Rao, *Phys. Rev. Lett.* **99**, 047403 (2007); N. Bonini, R. Rao, A. M. Rao, N. Marzari, and J. Menéndez, *Phys. Status Solidi B* **245**, 2149 (2008).
- <sup>21</sup>V. V. Deshpande, S. Hsieh, A. W. Bushmaker, M. Bockrath, and S. B. Cronin, *Phys. Rev. Lett.* **102**, 105501 (2009).
- <sup>22</sup>S. Datta, *Electronic Transport in Mesoscopic Systems* (Cambridge University Press, Cambridge, 1995).
- <sup>23</sup>H. Ishii, S. Roche, N. Kobayashi, and K. Hirose, *Phys. Rev. Lett.* **104**, 116801 (2010).
- <sup>24</sup>G. Pennington, S. J. Kilpatrick, and A. E. Wickenden, *Appl. Phys. Lett.* **93**, 093110 (2008).
- <sup>25</sup>N. Vandecasteele, M. Lazzeri, and F. Mauri, *Phys. Rev. Lett.* **102**, 196801 (2009).
- <sup>26</sup>H. Suzuura and T. Ando, *J. Phys. Soc. Jpn.* **77**, 044703 (2008).
- <sup>27</sup>V. V. Aristov, *Direct Methods for Solving the Boltzmann Equation and Study of Nonequilibrium Flows* (Kluwer Academic, Dordrecht, 2001).
- <sup>28</sup>We use a space and momentum grid with 500 points. The momentum range is then given by  $5eU/(\hbar v_F)$ .
- <sup>29</sup>N. Bonini, M. Lazzeri, N. Marzari, and F. Mauri, *Phys. Rev. Lett.* **99**, 176802 (2007).
- <sup>30</sup>S. Jursenas, A. Zukauskas, and R. Baltramiejunas, *J. Phys.: Condens. Matter* **4**, 9987 (1992).
- <sup>31</sup>S. P. Hepplestone and G. P. Srivastava, *Phys. Rev. B* **74**, 165420 (2006).
- <sup>32</sup>R. Saito, T. Takeya, T. Kimura, G. Dresselhaus, and M. S. Dresselhaus, *Phys. Rev. B* **57**, 4145 (1998).
- <sup>33</sup>G. D. Mahan, *Phys. Rev. B* **65**, 235402 (2002).
- <sup>34</sup>S. Zhang, M. Xia, S. Zhao, T. Xu, and E. Zhang, *Phys. Rev. B* **68**, 075415 (2003).
- <sup>35</sup>K. Ishikawa and T. Ando, *J. Phys. Soc. Jpn.* **75**, 084713 (2006).
- <sup>36</sup>H. Haug and A.-P. Jauho, *Quantum Kinetics in Transport and Optics of Semiconductors* (Springer, Heidelberg, 1998).
- <sup>37</sup>G. Baym and L. P. Kadanoff, *Phys. Rev.* **124**, 287 (1961).
- <sup>38</sup>M. S. Dresselhaus, G. Dresselhaus, R. Saito, and A. Jorio, *Phys. Rep.* **409**, 47 (2005).